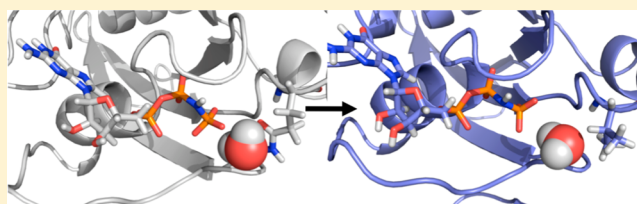# Electrostatic Effects of Mutations of Ras Glutamine 61 Measured Using Vibrational Spectroscopy of a Thiocyanate Probe

Amy J. Stafford, David M. Walker, and Lauren J. Webb*

Department of Chemistry and Biochemistry, Institute for Cell and Molecular Biology, and Center for Nano- and Molecular Science and Technology, The University of Texas at Austin, 1 University Station, A5300, Austin, Texas 78712, United States

ABSTRACT: Mutations of human oncoprotein p21[Ras] (hereafter Ras) at glutamine 61 are known to slow the rate of guanosine triphosphate (GTP) hydrolysis and transform healthy cells into malignant cells. It has been hypothesized that this glutamine plays a role in the intrinsic mechanism of GTP hydrolysis by interacting with an active site water molecule that electrostatically stabilizes the formation of the charged transition state at the γ-phosphate during hydrolysis. We have tested the interactions between amino acids at this position and water by measuring changes in the electrostatic field experienced by a nitrile probe positioned near Ras Q61 using vibrational Stark effect (VSE) spectroscopy. We mutated this glutamine to every amino acid except cysteine and proline and then incubated these mutants with a Ral guanine nucleotide dissociation stimulator (Ral) containing the I18C mutation that was chemically labeled with a thiocyanate vibrational spectroscopic probe. The formation of the docked Ras Q61X–labeled Ral complex was confirmed by measurement of the dissociation constant of the interaction. We measured the absorption energy of this nitrile to determine any differences in electrostatic environment in the immediate vicinity of the thiocyanate probe between wild type and mutants of Ras. For each Ras Q61X mutant, we correlate the change in electrostatic field at position 61 with the solvent accessible surface area of polar components of the mutant side chain determined from a Boltzmann-weighted ensemble of structures, as well as the residue's hydration potential. These results support the hypothesis that the role of Ras Q61 is to stabilize water in or near the active site during GTP hydrolysis. The substantial effect that nonpolar side chains of Ras Q61X have on the absorption energy of the thiocyanate must be investigated with further experiments.

Human oncoprotein p21[Ras] (Ras) is the canonical member of a superfamily of guanosine triphosphate (GTP)-hydrolyzing proteins that switch between an ON state when bound to GTP and an OFF state when bound to guanosine diphosphate (GDP) in the regulation of signal transduction pathways.[1] In the ON state, Ras binds to several downstream effectors for propagation of chemical signals that regulate cell division, cell survival, and apoptosis.[2–5] Two well-studied downstream effectors are c-Raf-1 (hereafter called Raf) and the Ras binding domain (RBD) of the Ral guanine nucleotide dissociation stimulator (hereafter called Ral). Mutations of Ras are found in approximately 30% of human cancer tumors;[1] several of these mutations are known to inhibit GTP hydrolysis, thus leaving the protein permanently in the ON state and causing uncontrolled cell division and cancer. This important role in the formation and growth of human cancers has made Ras a central focus of research in molecular oncology since its discovery in 1964.[6]

Most Ras mutants found in human cancer tumors are located at positions G12, G13, and Q61.[3,7–10] Glutamine 61 is of particular interest because of the role it is believed to play in the hydrolysis of GTP to GDP, a necessary step in switching Ras to the inactive OFF state. The intrinsic mechanism of GTP hydrolysis by Ras is slow; a physiologically relevant rate of hydrolysis occurs when Ras is activated by docking to the Ras GTPase activating protein (RasGAP). This places an arginine near the Ras active site, which increases the rate of hydrolysis of GTP by $\sim 10^5$.[11] The role of Q61 in this process is not fully understood, but studies of mutations at Q61 using crystallography,[12,13] kinetics,[14] and theoretical modeling[14,15] have indicated that the glutamine does not participate chemically in the hydrolysis reaction but instead is responsible for stabilizing the structural and electrostatic organization of the active site, which in turn allows the so-called "arginine finger" on RasGAP to stabilize a highly polar transition state caused by nucleophilic attack on the γ-phosphate of GTP.[13,15]

In recent years, attention has turned to determining the intrinsic mechanism of GTP hydrolysis performed by Ras in the absence of binding to RasGAP.[13] This is critically important because the dissociation constant of the Ras–Raf complex (3.5 nM)[13] is considerably lower than that of the Ras–RasGAP complex (1–100 μM),[16] and any therapeutic strategy targeted at mutated, carcinogenic versions of Ras will most commonly encounter the protein in a state in which it is docked with the downstream effector, not RasGAP. In both intrinsic and induced GTP hydrolysis, it is known that a water molecule acts as a general base to attack the γ-phosphate of GTP; this water molecule has been observed in several crystal structures of

catalytically active Ras.[13,17] The arginine finger of RasGAP appears to be able to stabilize the nucleophilic character of the transition state thus created.[10,15] It has been hypothesized that in the intrinsic mechanism of GTP hydrolysis, this stabilization function is conducted by a second appropriately placed water molecule in the active site, and that Q61 in turn stabilizes this second water molecule. This proposed mechanism is shown in Figure 1, where a catalytic water molecule shuttles a proton to a
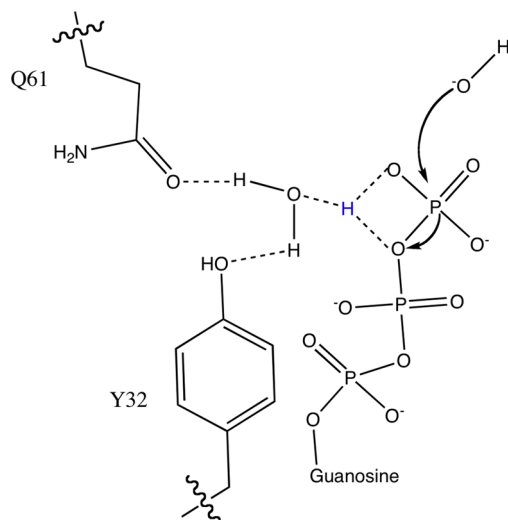

Figure 1. Proposed mechanism for intrinsic GTP hydrolysis by Ras, showing Q61 hydrogen bonding to a developing H_3O^+ formed from a proton (blue) transferred from a catalytic water molecule. Adopted from ref 13.

second water molecule (via the γ-phosphate), where it is stabilized by hydrogen bonding to the side chain of Q61. This hydronium ion creates a region of partial positive charge near the phosphate, which in turn stabilizes the growing negative charge on the dissociative transition state occurring at the γ-phosphate during hydrolysis. This hydronium ion thus fills a function in the intrinsic mechanism of GTP hydrolysis in Ras similar to that of the arginine finger of RasGAP in the induced mechanism of GTP hydrolysis.[13] This proposed mechanism has been supported by crystal structures of catalytically inactive Ras mutants that show either a different distribution of water near the γ-phosphate of GTP (Ras Q61G)[12] or a distribution in which this water molecule is missing altogether (Ras Q61L, Q61V, Q61K, and Q61I).[18,19] The positive charge on the hydronium ion would be stabilized to some degree by any polar component of any side chain, except perhaps the positively charged Lys and Arg residues (which may be able to fill this stabilization role themselves). Direct measurement of such stabilization between polar components of amino acid side chains and water molecules associated with the protein would further improve our understanding of the mechanisms of both intrinsic and induced GTP hydrolysis and allow the development of hypotheses for how the rate of these mechanisms could be altered by the introduction of outside chemical inputs. This capability could guide the development of drug candidates that would enhance the rate of hydrolysis in carcinogenic mutants of Ras by focusing on the Q61 side chain of the Ras−effector interface. Here, we propose that a necessary step in investigating this proposed mechanism involves a systematic study of how the side chain of Ras Q61X interacts noncovalently with water.

The noncovalent interaction between Q61 and water can be addressed with appropriately placed vibrational probes that have well-characterized shifts in absorption energy based on their exposure to water. Several useful probes have been identified for this investigation, including the carbon−deuterium bond,[20] the azide,[21] and the nitrile[22,23] vibrational stretching modes.[24] These probes are useful because they are in a clear region of the protein's vibrational spectrum (2000−2500 cm^{-1}) and, for the azide and nitrile groups, have reasonably high oscillator strengths.[22] Placing a vibrational probe such as a nitrile near Q61 would therefore be a convenient way of measuring the relative amount of water near that active site, allowing clarification and elucidation of the role of water near the Ras active site during GTP hydrolysis. Furthermore, the noncovalent interaction between Q61 and water will be dominated by perturbations in local electrostatic forces at the side chain−water interface. Because the large and heterogeneous electrostatic fields caused by the arrangement of amino acid partial charges in the protein's tertiary structure influence all aspects of protein function, including protein−protein interactions[25−30] and enzymatic catalysis,[31,32] there has been considerable interest in experimental methods that can measure such fields directly.[33−41] One recently developed technique for measuring the effect of electrostatic influences on protein function is vibrational Stark effect (VSE) spectroscopy, in which a local spectroscopic probe is used as an unobtrusive direct measurement of the role of electrostatic field in aspect of protein function.[23,31,32,42−44] In VSE spectroscopy, the response of a probe vibrational oscillator to its local electrostatic environment is measured spectroscopically and is used to quantitate the magnitude and direction of the local electric field to which the probe is exposed. After calibration, the probe is inserted into a known position of a protein where it becomes a local, sensitive, and directional reporter of fluctuations of the protein's electrostatic field caused by structural or chemical perturbations in the protein. Here, the term "vibrational Stark effect" refers to changes in the vibrational absorption spectrum of a calibrated vibrational probe when exposed to changes in local electrostatic field caused by environmental stimuli.[23,24] These measurements will then provide experimental data for comparison to calculations of transition state structures and energies for a full elucidation of enzymatic mechanisms.

Recent work in our laboratory has focused on measuring electrostatic fields at the interface of the RBD of Ral, an effector that is normally thought to interact most strongly with the GTP-bound state of the Ras-like protein Rap1A (hereafter Rap).[43,45] The RBD of Ral also binds with the GTP-bound state of Ras with a dissociation constant approximately one order of magnitude greater than that with Rap. The docked Ras−Ral complex has been characterized by a crystal structure.[46] We have constructed a comprehensive experimental map of electrostatic fields in the interfacial region formed by the binding of wild-type (WT) Ras to thiocyanate (SCN) VSE probes located on the surface of Ral.[43] In so doing, we accumulated a library of the binding behavior of SCN-labeled Ral variants with WT Ras and determined that the dissociation constant, K_d, of the docking interaction was not perturbed by the introduction of the SCN probe on Ral mutants into the binding interface. These results suggested to us that SCN-labeled Ral variants could be used as a tool to study the electrostatic basis of differences between WT Ras and known carcinogenic mutants, where structural and kinetic factors

involved in the docking interaction were controlled to the greatest extent possible. A crystal structure of Ras Q61G has been determined and shows that the binding interface [residues 24−42 (Figure 2)] is very similar to the WT protein (rmsd of
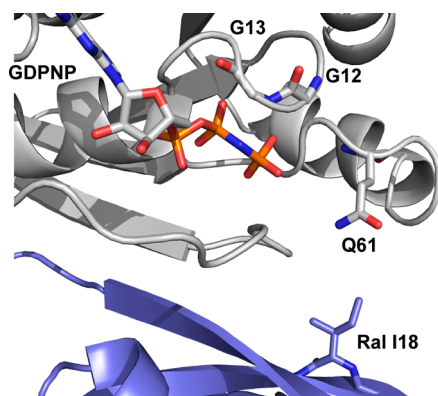

Figure 2. Crystal structure of the docked Ras (gray)−Ral (blue) complex highlighting amino acids G12, G13, and Q61 of Ras and I18 of Ral. Also shown is the nonhydrolyzable GTP analogue GDPNP bound to the active site of Ras. This figure was prepared from the crystal structure of PDB entry 1LFD.[46]

0.30 Å for all backbone atoms, rmsd of 0.31 Å for residues 24−42). Furthermore, when the Ras Q61G mutant was docked with the RBD of Raf, the free energy of association of the protein−protein interaction remained approximately constant.[12] Although no crystal structure of the docked mutant Ras−Raf complex is available, the similarity in structure and binding thermodynamics of the Q61G mutant with WT Ras is circumstantial evidence that the structures of the mutant Ras−Raf complexes are similar to that of the WT protein.[12] On this basis, we made the assumption that structures of the mutant Ras−Ral complexes were also similar to the WT structures observed in the crystal structure of Protein Data Bank (PDB) entry 1LFD.[46] A careful examination of this structure suggested to us that nitrile VSE probes inserted into the binding interface of the Ras−Ral docked complex could be used as a tool for placing electrostatic probes as close as possible to the functional areas of carcinogenic Ras Q61X mutants without introducing any structural or chemical changes into those regions, thereby allowing us to measure the electrostatic effects of mutations at position 61 from the perspective of the interface formed between Ras and its downstream effector. When Ras is docked with Ral, Ras Q61 is approximately 15 Å from Ral I18 [measured for the Cα atoms (Figure 2)]. Although this is a considerable distance, there is as yet no understanding of the effect on distance between the VSE probe and an electrostatic perturbation in the low-dielectric environment of a protein. Because of this, we believed that among our library of Ras-based SCN probes, the proximity of Ral I18 to Ras position 61 made it the most appropriate position for placing the VSE spectroscopic probe for investigation of electrostatic effects of mutations of Ras Q61.

In the study described here, we mutated Ras Q61 to every amino acid except cysteine and proline (which we have not successfully expressed and purified). We then bound these mutants to Ral I18C labeled with the nitrile VSE probe and, after confirming that the docked complex still formed through K_d measurements and gel filtration chromatography, measured the absorption energy of this nitrile to determine any differences in the electrostatic

environment of the nitrile probe caused by mutations at Ras Q61. Through molecular dynamics (MD) sampling, we generated a Boltzmann-weighted ensemble of structures of each Ras Q61X mutant docked with the nitrile-labeled variant of Ral I18C and measured the solvent accessible surface area (SASA) of each side chain at Ras Q61X. We correlate the change in the absorption energy of the thiocyanate probe based on mutations of Ras Q61 with the both the residue's SASA and the residue's hydration potential at pH 7. These results support the hypothesis that the role of Q61 is to stabilize water molecules in and near the active site of Ras during GTP hydrolysis.

■ MATERIALS AND METHODS

Protein Mutagenesis, Expression, and Purification. Amino acid mutations were made using the Quikchange mutagenesis kit (Stratagene) with polymerase chain reaction primers obtained from Sigma-Aldrich. The 97-residue RBD of Ral was taken from residues 790−886 of RalGDS.[47] For the sake of clarity, we adopt the numbering convention of a Ral crystal structure, PDB entry 1LFD,[46] which indexes the glycine at position 797 in Ral as G14. The residue index numbers in this work therefore correspond to PDB entry 1LFD. The gene was synthesized and cloned into the pET-15b expression vector (Novagen) by GenScript (Piscataway, NJ), and the sequence was confirmed. The C16A and C17A mutations were used to remove both wild-type cysteines, generating a protein construct with no cysteine residues that we hereafter call Ralβ. Finally, a cysteine was introduced at position 18 to generate the Ralβ I18C mutant. This construct was transformed into *Escherichia coli* strain BL21(DE3) (Novagen) for recombinant expression. A plasmid containing a hexahistidine-tagged tobacco etch virus protease (His-TEV) with the S219V mutation was obtained from Addgene (Addgene plasmid 8827) in *E. coli* strain BL21(DE3)-RIL.[48] The expression vector for WT H-Ras, residues 1−166, was a generous gift from the Kuriyan laboratory.[49] This gene was expressed in pProEX (Invitrogen) with a hexahistidine tag that was separated from the protein construct by a cleavage site for His-TEV. Plasmids encoding mutations at Ras Q61 were transformed into *E. coli* strain BL21(DE3) for recombinant expression. All proteins were expressed and purified as previously described.[43] After purification, Ras Q61X mutants were loaded with the nonhydrolyzable GTP analogue guanosine 5′-(β,γ-imido)-triphosphate trisodium salt hydrate (GDPNP, Sigma) to maintain the protein in the GTP-bound ON state. Yields for Ras Q61X mutants were typically 30−50 mg of protein/L of growth medium. The Ras Q61C and Q61P mutations could not be expressed for reasons that we have not investigated.

Introduction of the Nitrile Functional Group. The conversion of a cysteine thiol into the thiocyanate Stark probe was achieved by the reaction of Ralβ I18C with 2 molar equiv of 5,5′-dithiobis(2-nitrobenzoic acid) (DTNB, Sigma-Aldrich), which has been described previously.[42,43] The reaction mixture was incubated at room temperature for 2−14 h, forming the protein-bound thionitrobenzoic acid disulfide (PS-TNB). The extent of the reaction was monitored by observing the formation of the TNB⁻ side product by its absorption at 412 nm (ε_{412} = 13600 M⁻¹ cm⁻¹). After 1 equiv of TNB⁻ had been generated, 100 molar equiv of potassium cyanide (KCN) was added to displace the protein-bound TNB and generate the protein−thiocyanate complex (PS−CN). The extent of reaction was again observed by absorption of the TNB⁻ side product at 412 nm. At the end of the reaction, a PD-10 desalting

column (GE Healthcare) was used to remove excess TNB$^-$ and CN$^-$ and return the labeled protein to labeling buffer [50 mM Tris (pH 7.5) and 100 mM NaCl]. In most cases, electrospray ionization mass spectrometry (ESI-MS) was used to confirm the addition of 26 Da to the mass of the purified protein, indicating the presence of the SCN label. The SCN-labeled Ralβ construct is hereafter termed Ralβ I18C$_{SCN}$.

Kinetic Analysis of Ralβ I18C$_{SCN}$ Docked to WT Ras and Ras Q61X Mutants. The docked complex of either WT Ras or a Ras Q61X mutant with Ralβ I18C$_{SCN}$ was formed by incubating the SCN-labeled Ralβ with 2 molar equiv of the desired Ras mutant at 4 °C for up to 16 h. Gel filtration chromatography [Superdex 200 (GE Healthcare) equilibrated in labeling buffer] was used to confirm the formation of the docked complex at ~31 kDa using both WT Ras and several Q61X mutants. The dissociation constant, K_d, of the interaction was measured using a guanine nucleotide dissociation inhibition (GDI) assay described previously.[50] WT Ras (100 nM) or Ras Q61X (100 nM) bound to the fluorescently labeled GTP 2′(or 3′)-O-(N-methylanthraniloyl)guanosine 5′-triphosphate trisodium salt (mant-GTP, Invitrogen) was incubated with varying concentrations of Ralβ I18C$_{SCN}$ at 37 °C for 1−2 h in a black 96-flat well plate (Microfluor 1, Thermo Scientific). The dissociation of mant-GTP was initiated by the addition of 250 mM GDPNP, and the plate was quickly inserted into a fluorometer and shaken for 30 s to mix the solution. The decay of the fluorescence of mant-GTP was monitored in a multimode detector (Beckman-Coulter, DTX 800) using top-down intensity. The detector was set with excitation and emission wavelengths of 365 and 450 nm, respectively. The initial rate of this decay was taken to be the observed rate of the dissociation reaction, k_{obs}. This was fit to eq 1 to determine the dissociation constant, K_d:

$$k_{obs} = k_{-1} - k_{-1}$$
$$\times \frac{R_0 + E_0 + K_d - \sqrt{(R_0 + E_0 + K_d)^2 - 4R_0E_0}}{2R_0}$$

$$(1)$$

where R_0 is the concentration of WT Ras or Ras Q61X, E_0 is the concentration of Ralβ I18C$_{SCN}$, and k_{-1} is the rate constant for dissociation of mant-GTP from Ras in the absence of the RBD.[50]

Vibrational Spectroscopy. Infrared spectra of the docked Ras Q61X−Ralβ I18C$_{SCN}$ complex were recorded in labeling buffer as previously reported.[43] Ralβ I18C$_{SCN}$ was incubated with 2 molar equiv of a Ras Q61X mutant at 4 °C overnight. The solution was then concentrated by centrifugation to approximately 2 mM. Vibrational absorption spectra were recorded at room temperature in a sample cell composed of two sapphire windows separated by 125 μm thick PETE spacers in a Bruker Vertex 70 FTIR instrument. The sample cell was illuminated with light in the range of 2000−2500 cm^{-1} selected by a broad bandpass filter (Spectrogon, Parsippany, NJ) placed in front of the instrument's IR source. Spectra were composed of 250 scans collected with a liquid nitrogen-cooled indium antimonide (InSb) detector at 0.5 cm^{-1} spectral resolution. The background-subtracted spectra were fit to a Gaussian line shape with a custom least-squares fitting program to determine the peak center, ν_{obs}, and the full width at half-maximum (fwhm). Uncertainty in absorption energy is reported as the standard deviation of at least five measurements.

The observed change in the absorption energy of the thiocyanate, $\Delta\nu_{obs}$, versus WT Ras was then related to the change in the electrostatic field projected onto the nitrile bond axis caused by the mutation of Ras Q61, $\Delta\vec{F}_{Q61X}$, through eq 2:

$$\Delta E = hc\Delta\nu_{obs} = -\Delta\vec{\mu}_{SCN}\cdot\Delta\vec{F}_{Q61X} \qquad (2)$$

The difference dipole moment ($\Delta\vec{\mu}_{SCN}$), also called the Stark tuning rate, has been previously measured to be 0.7 cm^{-1}/(MV cm)[42] (i.e., a 1 MV/cm increase in electrostatic field upon docking will shift the absorption energy of the thiocyanate probe by −0.7 cm^{-1}). This dipole vector is taken to point from the nitrogen atom to the carbon atom of the thiocyanate.[51]

Molecular Dynamics Simulations and Solvent Accessible Surface Area Calculations. A model for WT Ras docked with the cyanocysteine-containing downstream effector Ralβ I18C$_{SCN}$ was constructed as described previously.[45] With this model, we generated 15 mutations at position 61 of Ras; mutations to alanine and glycine were not sampled because they lack a χ_1 angle (see below), and cysteine and proline were not sampled because of the lack of experimental data. These mutations were introduced using the tleap utility in AMBER tools using a ffamber03 force field[52] with a parametrized cyanocysteine residue as discussed previously.[43,45] This generated 16 structures of each Ras Q61X mutant (including WT Ras) docked with Ralβ I18C$_{SCN}$.

Each of the models was then subjected to initial vacuum energy minimizations, using 100 steps of steepest decent integration in the GROMACS utility mdrun.[53] These energy-minimized structures were then subjected to torsional biasing by generating six rotamer models 60° apart about the χ_1 dihedral angle (N−Cα−Cβ−Cγ) for each reside at position 61 of Ras. Each of these torsions was sampled using dihedral restraints centered about the angle of interest that were flat within 45° and with a quadratic force constant of 1000 kJ mol^{-1} rad^{-2} outside of that range. This generated a total of six structures for each Ras Q61X mutant. Each of these structures was solvated with tip3p water.[54] Charge neutralization with sodium ions, solvent equilibration, and molecular dynamics sampling were conducted as described previously.[43,45] Three 1 ns trajectories were generated for each rotamer using the mdrun utility in GROMACS for a total sampling time of 18 ns per construct. The Boltzmann weighted torsional distributions for the χ_1 dihedral for position 61 of Ras were calculated using a weighted histogram analysis method (WHAM).[55,56] The torsional distribution of the side chain for the last 12 ns of simulation time was compared to that compiled from the first 6 ns and showed essentially identical WHAM-derived probabilities for side chain distribution, indicating that the simulation had fully converged (data not shown).

The SASA for each sampled residue at position 61 of Ras was calculated using the g_sas utility in GROMACS on each of the trajectories generated during the molecular dynamics sampling. The output was then Boltzmann weighted using the torsional distributions calculated previously. SASAs were calculated using either the entire residue (including backbone atoms), only side chain atoms, or only atoms that can participate in hydrogen bonding for either the entire residue or the side chain only. In the following discussion, the atoms that can participate in hydrogen bonding (oxygen, nitrogen, and hydrogen atoms bonded to them) are termed polar atoms.

■ RESULTS AND DISCUSSION

Formation of the Mutant Ras Q61X−Ralβ I18C$_{SCN}$ Docked Complex. We have shown previously that the dissociation constant of the docked Ras−Ral complex is not altered by the introduction of the thiocyanate probe through chemical labeling of Ralβ I18C$_{SCN}$. The dissociation constants, K_d, measured for docking of WT Ras with both WT Ral and Ralβ I18C$_{SCN}$ are identical (2.7 ± 0.2 and 2.6 ± 0.2 μM, respectively).[43] Docking between Ras Q61X mutants and Ralβ I18C$_{SCN}$ was further confirmed via gel filtration studies, in which Ralβ I18C$_{SCN}$ formed a docked complex at ∼31 kDa with both WT Ras and several Ras Q61X mutants. K_d values of Ralβ I18C$_{SCN}$ with 17 mutants of Ras Q61X are listed in Table 1.

Table 1. Dissociation Constants of Ralβ I18C$_{SCN}$ Docked to WT Ras and Ras Q61X Mutants[a]

	K_d (μM)
WT	2.6 ± 0.2
Q61A	18.8 ± 0.7
Q61D	13.0 ± 0.6
Q61E	11.7 ± 0.4
Q61F	36.2 ± 0.8
Q61G	8.8 ± 0.3
Q61H	22.2 ± 0.2
Q61I	7.0 ± 0.6
Q61K	4.1 ± 0.7
Q61L	2.4 ± 0.3
Q61M	7.8 ± 0.3
Q61N	2.6 ± 0.2
Q61R	15.9 ± 0.7
Q61S	20.4 ± 0.9
Q61T	28.1 ± 0.7
Q61V	5.9 ± 0.9
Q61W	39.6 ± 1.0
Q61Y	31.7 ± 0.8

[a]The error is reported as one standard deviation of at least three independent measurements.

Several of these mutations do indeed effect protein−protein docking interaction, with mutations to Phe, His, Ser, Thr, Trp, and Tyr causing an increase in the protein−protein dissociation constant by a factor of as much as ∼10, to 20−36 μM. However, none of these mutations are associated with a particularly large increase in the fwhm of the absorption spectrum of the docked complex relative to that of WT Ras (see Table 2). A significantly larger fwhm has been qualitatively associated with increased conformational freedom of the thiocyanate, which could be caused by slow or unstable binding of the nitrile-containing protein to Ras Q61X mutants to form the interface of interest.[23] The relatively constant fwhm is not surprising, given that under the conditions in which the IR spectra were collected, even with a dissociation constant of 10 μM, at least 90% of the sample will be in the docked configuration, assuming simple steady state kinetics. The kinetic data therefore demonstrate that there is no significant disruption in the Ras Q61X−Ral I18C$_{SCN}$ interface caused by the mutations and thiocyanate labeling employed in this study.

VSE Spectroscopy of Ras Q61X−Ralβ I18C$_{SCN}$ Complexes. Representative examples of VSE spectra of the SCN probe on Ralβ I18C$_{SCN}$ docked with both WT Ras and Ras Q61T are shown in Figure 3. When on the surface of the monomer, the thiocyanate on Ralβ I18C$_{SCN}$ was found to

absorb at 2163.1 ± 0.3 cm^{-1} with a fwhm of 12.1 ± 0.5 cm^{-1}. The absorption energy of the probe decreases slightly when the system goes from the monomeric to docked complexes, but with no significant difference in fwhm, as reported previously.[43] The absorption energies of the thiocyanate on Ralβ I18C$_{SCN}$ docked with each Ras Q61X mutant are compiled in Table 2 and demonstrate that certain amino acid substitutions at position 61 do indeed cause a change in the absorption energy of the thiocyanate, demonstrating a change in the electrostatic environment in the vicinity of the thiocyanate. Although these shifts are small, so are the error bars, and the trends suggested in Table 2 are clear. We used these data to test the influence that various side chain characteristics have on the change in the electrostatic environment experienced by the probe. We first tested the correlation between the absorption energy of the thiocyanate probe when docked to each Ras Q61X mutant relative to WT and the measured K_d of the docking interaction but found only a weak correlation between the two [r = 0.34 (data not shown)]. Below, we reexamine this finding in light of the effects of side chain polarity on the observed interaction.

Because we are interested in determining the extent of the ability of side chain mutations at position 61 to stabilize a water molecule that could be involved in intrinsic GTP hydrolysis by Ras, we selected two measurements of the affinity of the amino acid side chain for water: SASA of the polar components of the side chain and hydration potential. The calculated SASAs for the entire residue (including backbone atoms), the entire side chain, and only the polar components of the amino acid capable of participating in hydrogen bonding are listed in Table 3. These values were determined by assembling a Boltzmann-weighted ensemble of structures of each Ras Q61X mutant docked with Ralβ I18C$_{SCN}$ and thus specifically took into account any steric occlusion of water molecules around position 61 from nearby amino acid residues on either Ras or Ralβ I18C$_{SCN}$. We compared our calculated polar SASAs to those previously reported by Wimley et al., calculated for peptides AcWL-X-LL and AcGG-X-GG (where X was each amino acid),[57] and found a correlation between the two values (r = 0.84). We report the SASAs determined from our Boltzmann-weighted ensemble of Ras Q61X−Ralβ I18C$_{SCN}$ structures because they most accurately reflect our experimental system. These data are an estimate of the extent to which the polar, hydrophilic component of each residue interacts with water.

The relationship between the polar SASA of each amino acid side chain and the measured absorption energy of our thiocyanate probe when docked with each Ras Q61X mutant is shown in Figure 4. (Although we did not simulate Ras Q61A or Q61G, they are included in the figure because they have no polar atoms in their side chain, and thus, the value of the polar SASA for each residue is 0.) The correlation between Ras Q61X mutants with non-zero polar SASAs and the observed absorption energy of the thiocyanate on Ralβ I18C$_{SCN}$ was found to be r = 0.72. The correlation between the side chain surface area and absorption energy was not simply steric; a plot of the total side chain SASA versus the observed vibrational absorption energy for each Ras Q61X mutant was essentially random [r = 0.1 (data not shown)]. As the polar SASA decreases, the orientation and kinetic behavior of water near the side chain at position 61 changes, altering the electric field at the protein−protein interface to which our vibrational probe is exposed. The effect of the extent of hydrogen bonding from the side chain at position 61 of Ras to water can therefore be

Table 2. Measured SCN Vibrational Frequencies (ν_{obs}) of Ralβ I18C$_{SCN}$ Docked with WT Ras and Ras Q61X Mutants, Measured Differences in Absorption ($\Delta\nu_{obs}$) and Field ($\Delta\vec{F}_{Q61X}$) of Ras Q61X Mutants versus WT Ras, Measured Full Widths at Half-Maximum (fwhm) of Ralβ I18C$_{SCN}$ Docked with WT Ras and Ras Q61X Mutants, and Differences (Δfwhm) between Ras Q61X Mutants and WT Ras[a]

form of Ras to which Ralβ I18C$_{SCN}$ is bound	ν_{obs} (cm^{-1})	$\Delta\nu_{obs}$ relative to WT Ras (cm^{-1})	$\Delta\vec{F}_{Q61X}$ (MV/cm)	fwhm (cm^{-1})	Δfwhm (cm^{-1})
WT Ras	2162.8 ± 0.2	0.0	0.0	12.8 ± 0.5	0.0
Residues with Some Hydrophilic Character					
Ras Q61D	2162.0 ± 0.1	−0.8 ± 0.2	1.1	13.9 ± 0.1	1.1
Ras Q61R	2162.4 ± 0.1	−0.4 ± 0.2	0.6	14.6 ± 0.1	1.8
Ras Q61N	2162.7 ± 0.2	−0.1 ± 0.3	0.1	13.2 ± 0.2	0.4
Ras Q61E	2162.8 ± 0.2	0.0 ± 0.3	0.0	12.8 ± 0.7	0.0
Ras Q61K	2163.1 ± 0.3	0.3 ± 0.3	−0.4	12.8 ± 0.3	0.0
Ras Q61Y	2163.5 ± 0.1	0.7 ± 0.2	−1.0	13.9 ± 0.2	1.1
Ras Q61H	2163.8 ± 0.2	1.0 ± 0.3	−1.4	13.6 ± 0.4	0.8
Ras Q61W	2164.1 ± 0.2	1.3 ± 0.3	−1.9	13.7 ± 0.2	0.9
Ras Q61S	2164.4 ± 0.1	1.6 ± 0.2	−2.3	13.4 ± 0.3	0.6
Ras Q61T	2164.7 ± 0.2	1.9 ± 0.3	−2.7	12.4 ± 0.3	−0.4
Residues with No Hydrophilic Character					
Ras Q61A	2162.0 ± 0.2	−0.8 ± 0.3	1.1	13.4 ± 0.4	0.6
Ras Q61M	2162.6 ± 0.1	−0.2 ± 0.2	0.3	13.6 ± 0.1	0.8
Ras Q61F	2163.0 ± 0.2	0.2 ± 0.3	−0.3	13.6 ± 0.2	0.8
Ras Q61G	2163.1 ± 0.1	0.3 ± 0.2	−0.4	13.8 ± 0.6	1.0
Ras Q61L	2163.2 ± 0.2	0.4 ± 0.3	−0.6	12.0 ± 0.6	−0.8
Ras Q61V	2163.9 ± 0.0	1.1 ± 0.2	−1.6	14.2 ± 0.2	1.4
Ras Q61I	2164.0 ± 0.2	1.2 ± 0.3	−1.7	13.1 ± 0.1	0.3

[a]The error in ν_{obs} and fwhm is one standard deviation from multiple experiments. The error in $\Delta\nu_{obs}$ is linearly propagated error from the measurement of WT Ras vs Ras Q61X.
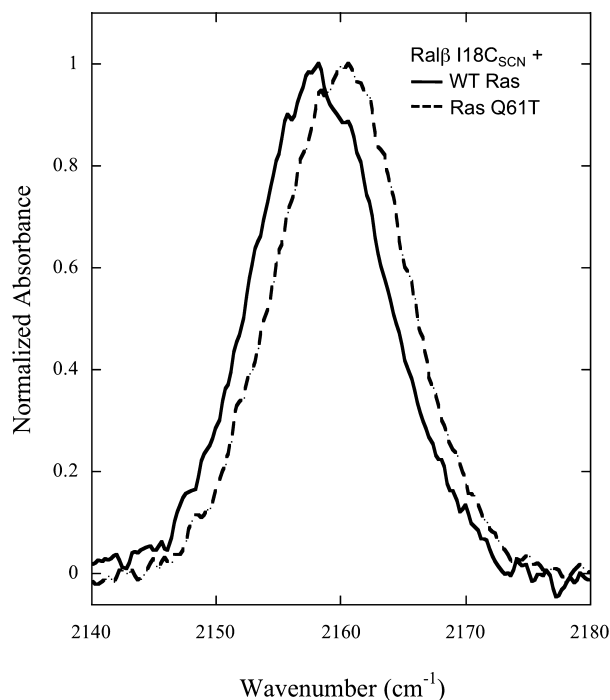

Figure 3. Normalized absorbance of thiocyanate on Ralβ I18C$_{SCN}$ measured when docked with WT Ras (—) (ν_{obs} = 2162.8 cm^{-1}) and Ras Q61T (---) (ν_{obs} = 2164.7 cm^{-1}).

interpreted as a Stark shift caused by the relative exposure of the thiocyanate probe to the electrostatic field generated at the protein−protein interface, which will differ on the basis of the chemical identity of the side chain. The negative slope of the correlation in Figure 4 implies that absorption energy of the

Table 3. Calculated SASAs for Amino Acids at Position 61 in Ras Q61X Mutants from Boltzmann-Weighted (χ1) Torsional Distributions[a]

form of Ras to which Ralβ I18C$_{SCN}$ is bound	SASA (Å^2)			
	entire residue	side chain	all polar atoms	side chain polar atoms
WT Ras	250 ± 10	179 ± 7	230 ± 17	114 ± 4
Residues with Some Hydrophilic Character				
Ras Q61D	216 ± 7	150 ± 6	200 ± 12	110 ± 4
Ras Q61R	290 ± 11	226 ± 8	144 ± 6	144 ± 6
Ras Q61N	222 ± 9	154 ± 6	210 ± 20	114 ± 4
Ras Q61E	242 ± 9	175 ± 6	230 ± 10	109 ± 5
Ras Q61K	260 ± 10	198 ± 8	202 ± 7	82 ± 2
Ras Q61Y	290 ± 10	230 ± 10	198 ± 4	77 ± 1
Ras Q61H	260 ± 10	191 ± 8	220 ± 20	114 ± 5
Ras Q61W	330 ± 20	270 ± 20	198 ± 7	80 ± 1
Ras Q61S	187 ± 6	118 ± 4	166 ± 8	77 ± 1
Ras Q61T	209 ± 7	145 ± 5	162 ± 7	77 ± 1
Residues with No Hydrophilic Character				
Ras Q61M	261 ± 10	194 ± 5	121 ± 3	0 ± 0
Ras Q61F	280 ± 10	220 ± 10	122 ± 3	0 ± 0
Ras Q61L	244 ± 9	182 ± 5	121 ± 3	0 ± 0
Ras Q61V	220 ± 7	159 ± 5	121 ± 3	0 ± 0
Ras Q61I	242 ± 8	183 ± 6	121 ± 3	0 ± 0

[a]Entire residue includes all of the atoms in the calculations; side chain includes only atoms from the side chain, and polar atoms are nitrogens, oxygens, and any hydrogens bonded to them. The error is reported as one standard deviation from the SASA calculation preformed on the 16 structures of the Boltzmann-weighted ensemble.

thiocyanate increased as the ability of the side chain to interact with water decreased. The strength of this correlation suggests
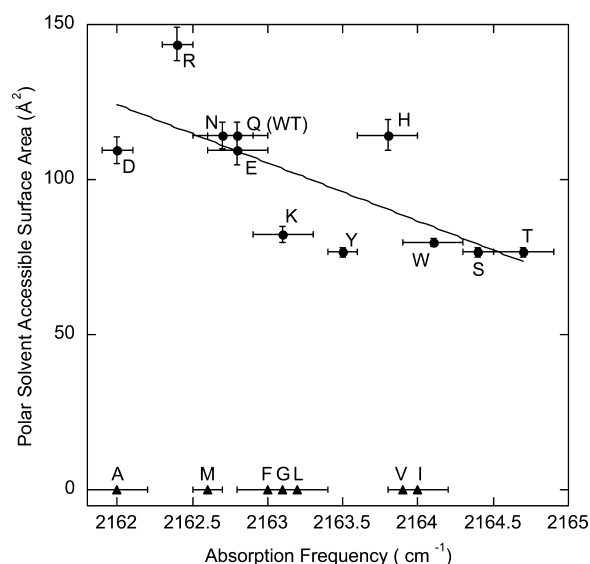
Figure 4. Solvent accessible surface area of polar side chain components compiled from molecular dynamics trajectories of Ras Q61X mutants vs the measured ν_{obs} of Ralβ I18C$_{SCN}$ docked with the Ras Q61X mutants: (●) hydrophilic residues and (▲) hydrophobic residues. The correlation for hydrophilic residues is $r = 0.72$. Error bars on ν_{obs} represent one standard deviation from multiple measurements. Error bars on SASA measurements represent one standard deviation of a Boltzmann-weighted ensemble of 18 ns of molecular dynamics trajectories for each Ras Q61X mutant.

that changes in the electrostatic environment of the probe can be related directly to the ability of each side chain at Ras Q61X to interact with water.

As discussed above, there was only a weak correlation between the measured dissociation constant of the Ras Q61X–Ralβ I18C$_{SCN}$ complex and the thiocyanate absorption energy. However, four of the six residues that caused the largest increase in the K_d of the docked complex (Ser, Thr, Trp, and Tyr) also displayed the four smallest polar SASAs. This raises the possibility that the changes in measured absorption energies of the thiocyanate caused by the mutations to these residues at Ras Q61X could be a convolution of both electrostatics and differences in docking of the GTPase with the downstream effector. To the best of our knowledge, there is no crystal structure of Ras containing any of these residues at position 61, and therefore, we cannot evaluate this possibility from the structural evidence. A structural change large enough to disrupt docking of the two proteins would likely not be observed in our MD trajectories, which were designed to assemble a Boltzmann-weighted ensemble of rotamers of Ras Q61X. However, we were able to use our MD simulations to test for significant local backbone and side chain motions at position 61 in each Ras Q61X mutant. As discussed extensively below, except for a small increase in the backbone rmsd of the region containing residue 61 for nonpolar side chains compared to polar side chains, no large or systematic structural changes were observed. Other simulations and experiments will be needed to determine the cause of the systematic effect of nonpolar or only slightly polar residues on the observed vibrational absorption energy.

To confirm that we are observing an effect of water near the thiocyanate probe, we also tested our measured vibrational absorption energy data against the hydration potential of the side chain at Ras Q61X. This quantifies the free energy of
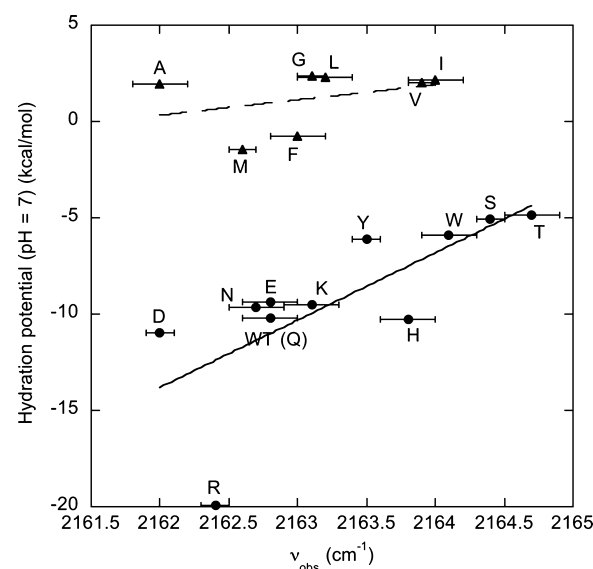

Figure 5. Hydration potentials for amino acid side chains compiled from ref 54 vs measured ν_{obs} values of Ralβ I18C$_{SCN}$ docked with Ras Q61X mutants: (●) hydrophilic residues (—) ($r = 0.72$) and (▲) hydrophobic residues (– – –) ($r = 0.34$). Error bars on ν_{obs} values represent one standard deviation from multiple measurements.

transfer of the side chain from the vapor phase to buffered water and is another common measurement of affinity for interactions with water. In Figure 5, we compare hydration potentials tabulated at pH 7 by Wolfenden et al.,[58] to our measured ν_{obs} values for each Ras Q61X mutation. As in Figure 4, we have divided the data into mutants composed of polar versus nonpolar residues. When considering polar residues, the correlation between hydration potential and absorption energy was found to be $r = 0.72$. When the outlier Arg was excluded from the least-squares fit, $r = 0.86$. When only the nonpolar residues are considered, there is a much smaller correlation between the hydration potential and vibrational absorption energy ($r = 0.34$). This is largely because the hydration potential of these residues varies over a range of only <4 kcal/mol, whereas the polar residues vary over a larger range, approximately 15 kcal/mol. For both polar and nonpolar residues, the absorption energy increases with increasing hydration potential, i.e., increasingly unfavorable interactions between the side chain and water. Thus, although the slopes of the correlations in Figures 4 and 5 are different, in both cases the absorption energy of the thiocyanate probe increases as the ability of the side chain at position 61 to interact favorably with water decreases, altering the electrostatic field at the protein–water interface.

In our previous work describing 11 thiocyanate probe locations on the surface of Ralβ, we measured a significant difference in the absorption energy of the vibrational probe based on its position on the surface of the monomeric, un-docked protein. Using molecular dynamics sampling, we generated a Boltzmann-weighted ensemble of structures of each SCN-labeled Ralβ mutant and measured the total SASA of each thiocyanate probe. We found that the absorption energy increased as the SASA decreased, i.e., as the probe was exposed to less water.[43] This was interpreted as a Stark shift caused by the relative exposure of each probe to the electrostatic field generated at the protein–water interface that differed on the basis of the exposure of a probe at each location to water. By

correlating the change in absorption energy of the thiocyanate probe at Ralβ I18C$_{SCN}$ in this study with two measures of water affinity, the polar SASA and hydration potential of the residue, we have now observed that the thiocyanate probe responds in a consistent way to the local electrostatic environment acting to stabilize or destabilize the presence of water. Further simulations in our laboratory are focusing on quantifying how Ras Q61X mutations alter the position and possible hydrogen bonding of water molecules near that side chain, not just their presence.

Polarity is a complex chemical phenomenon generated by molecular multipole moments and influences numerous measurable parameters such as solvation free energy, hydrogen bonding ability, solvent interactions, and reactivity. Polarity is a particularly important concept at position 61 of Ras because of previous experimental and computational studies that have linked the glutamine at that position to the ability of Ras to stabilize a water molecule near or in its active site, which in turn influences the rate of GTP hydrolysis through both intrinsic and induced mechanisms. The value of examining this phenomenon with a vibrational probe that is sensitive to electrostatic fields, such as the thiocyanate, is that the measured change in vibrational absorption energy can be directly correlated to a change in the electrostatic environment of the probe caused by mutations at Ras Q61 and projected onto the probe bond, $\Delta \vec{F}_{Q61X}$. The measured values of $\Delta \vec{F}_{Q61X}$ are listed in Table 2, ranked from largest positive to largest negative shift. While two charged residues with non-zero polar surface areas (Arg and Asp) increased the local electrostatic field of the probe (and Asn led to a negligible change), all other polar residues caused a decrease in the local electrostatic field of up to −2.7 MV/cm. For the amino acids with no nonpolar surface area, although the trend of decreasing field was also observed, there was a significantly lower correlation of this effect to the hydration potential of these residues [dashed line in Figure 5 ($r = 0.34$)] and no correlation to size or steric parameters (Figure 4).

Molecular Dynamics Simulations of Ras Q61X−Ralβ I18C$_{SCN}$ Complexes. Any significant structural change of amino acids in the vicinity of the nitrile probe would make comparison of vibrational energy differences between polar and nonpolar residues difficult. Furthermore, interpreting the presence of water molecules in and near the Ras active site is valid only when the protein is in a catalytic configuration. Because this occurs when Ras is docked to a downstream effector, our extensive Boltzmann-weighted molecular dynamics sampling could provide some clues about a structural basis for differences between polar and nonpolar residues. We used these structures to investigate three structural parameters: (1) rmsd of the backbone in the loop region containing Q61X (residues 59−62) compared to residues in an α-helix far from this site, (2) the angle of the side chain at position 61 with respect to the Ras−Ral interfacial plane, and (3) the orientation of the side chain with respect to an axis perpendicular to the surface plane containing both Ras Q61X and Ralβ I18C$_{SCN}$.

Residue 61 lies in a loop region of the Ras structure and therefore could be more prone to structural rearrangement upon mutagenesis. Because our MD simulation strategy resulted in converged structures after 18 ns of simulation time, we tested the rmsd of backbone atoms for the loop region, residues 59−62, compared with that of four residues residing in a stable α-helix far from this site, residues 92−95. Although the rmsd of the loop region, 0.33 ± 0.03 Å, was slightly larger than that of the control region, 0.22 ± 0.01 Å, this is still too small to sug-

gest that there is large scale rearrangement of the backbone caused by mutations at Ras Q61. There was, however, a trend toward a higher rmsd of nonpolar residues at position 61 (0.35 ± 0.03 Å) compared with that of the polar residues (0.32 ± 0.02 Å) that was not observed at the control position. Although these fluctuations are still small, along with the generally higher K_d values for nonpolar residues, they are further indication that nonpolar side chains at position 61 may lead to structural changes in that part of the protein. This in turn raises the possibility that the thiocyanate probe is in an entirely different location with respect to the surface of Ras and any surrounding water molecules, and thus that its vibrational absorption energy is influenced by factors other than simply a change in the electrostatic environment around Ras Q61X. Our use of this model system for studying electrostatic effects of Ras Q61X mutations on GTP hydrolysis is only valid when structural differences between the WT and mutant proteins are negligible. Any convolution of electrostatics with structural changes cannot be interpreted through the experiments that we describe here. Although the data in Figure 5 suggest that even these nonpolar residues respond similarly to polar residues when the hydration potential of the side chain is altered, further experiments are needed to verify that changes in the thiocyanate vibrational absorption energy caused by nonpolar residues at position 61 are not being influenced by large scale structural changes of the docked complex.

Although the backbone of Ras appears to be stable, it is possible that the orientation of the side chain at position 61 could change dramatically depending on the mutant. To investigate this, we defined two parameters for each side chain, equivalent to polar (ϕ) and azimuthal (θ) angles in spherical polar coordinates. The mathematical definitions of these two angles have been introduced extensively elsewhere;[45] we do not belabor those definitions here because we measured essentially no differences in these two structural parameters for any side chain at position 61 of Ras. The sole exception to this was a rotation of the indole group of Ras Q61W to relieve steric repulsions between the Trp side chain and the GDPNP nucleotide. No other significant structural motions were observed in our molecular dynamics sampling of torsional motions at this location.

Finally, it is possible that the thiocyanate at Ralβ I18C$_{SCN}$ behaves very differently when docked with Ras Q61X mutants than with WT Ras. We are not currently able to address this question because our simulations were designed to generate a Boltzmann-weighted ensemble of structures of the side chain at position 61 of Ras, not of the thiocyanate VSE probe. Because of this, questions about the relative orientation of the thiocyanate and the side chain at Ras position 61 or about changes in the SASA around the VSE probe caused by mutations at Ras Q61 cannot be addressed with our current MD sampling. Because of the implications of these results, accumulating such structures will clearly be important for further experimentation on Ras Q61X and is underway in our laboratory.

Implications for the Mechanism of Intrinsic GTP Hydrolysis. The role of Q61 in stabilizing a complex steric and electrostatic environment has previously been studied by Shurki et al.,[15] who found that the structure of glutamine at that position was essential for preserving the catalytic activity of induced GTP hydrolysis in the Ras−RasGAP complex. This study highlighted two key features of Q61, which have been confirmed by the experiments reported here. First, the structural differences between Ras in an unbound, monomeric

state and in the docked Ras—RasGAP complex are particularly large for residues 57—61. Buhrman et al.[13] have confirmed that any study of intrinsic GTP hydrolysis by Ras can only be properly studied when this region of the protein is in the catalytic configuration, such as when docked with a downstream effector protein that organizes this region. Thus, the downstream effector Ralβ I18C$_{SCN}$ used here to position the VSE probe close to Ras Q61 is also responsible for structurally organizing the active site into the catalytically relevant position. When a recent crystal structure of this ordered region (PDB entry 3K8Y)[13] is compared to the structure of Ras docked with the RBD of WT Ral (PDB entry 1LFD),[46] the backbone rmsd is 0.31 Å, while the backbone rmsd of the entire system is 0.31 Å, demonstrating that docking with the Ral downstream effector results in the correct structure for catalytic activity.[13] Second, Shurki and co-workers highlighted the structural importance of Q61 in promoting catalysis.[15] It is interesting that the only mutated residue at position 61 that produced no change in the absorption energy of the SCN probe was glutamate (Table 2), which although it is charged, is similar structurally to glutamine and has similar polar and nonpolar surface areas (Table 3).[57]

Furthermore, it has been proposed that useful information about how substitutions of Q61 affect the mechanism of hydrolysis must be studied when the complex is bound to a downstream effector such as Ral or Raf, in which the catalytic structure of Q61 is stabilized.[19] A systematic study of the effect of mutations at this site on the rate of hydrolysis of GTP while it is bound to the SCN-containing downstream effector will allow this chemical behavior to be correlated to the electrostatic environment of any stabilizing versus destabilizing mutation at position 61 and the possibility that the enzyme may be able to accommodate some changes in polarity and still function. Preparations are underway in our laboratory to connect the measurement of local electrostatic field based on each Q61X mutation to overall catalytic function of the protein by monitoring the rate of GTP hydrolysis, K_{cat}.[14,59−61] An early qualitative study of the mechanism of hydrolysis by Ras found that most mutations of Q61 result in approximately 10-fold lower rates of GTP hydrolysis, although no exact rate constants were measured.[62] Specific hydrolysis rate constants for several mutations of Q61 have been measured and have shown that Q61L, Q61I, and Q61K all result in slower GTP hydrolysis, while Q61E has actually been observed to accelerate GTP hydrolysis.[14,19] The fact that the charged lysine and hydrophobic leucine and isoleucine all cause a decrease in the rate of GTP hydrolysis demonstrates that the influence on GTP hydrolysis is more subtle than just the presence or absence of charge at that position. We believe that systematic examination of the VSE, K_d, and K_{cat} data of each Q61X mutant, particularly residues Arg, Asp, and Asn, which have the greatest polar surface area, will lead to a deeper understanding of this complex system. This will also allow us to connect the results described here with the effect of mutations to Ala and Gly at position 61, for which we were not able to generate a statistically weighted ensemble of structures. This will be presented in a future report.

Relevance of the Ras—Ral Interface in Studying GTP Hydrolysis. Measuring the electrostatic effects of mutations at Ras Q61 with a SCN probe in the Ras—Ral docked configuration is relevant to understanding the carcinogenic state of Ras for two reasons. First, as discussed above, the structural configuration of the active site that leads to productive hydrolysis in WT Ras can be induced by docking with the downstream

effector Raf, which we have assumed also extends to Ral. Shurki and co-workers[15] have meticulously described the importance of this structural configuration for any fundamental understanding of GTP hydrolysis by Ras. This configuration, conveniently, is induced by docking to the downstream effector.[13] The experiments described here confirm the importance of this residue in interacting with water near and in the active site, as suggested by previous crystallographic data, but using a technique which can be applied to measuring directly the magnitude of the electrostatic field caused by changes in the composition of the protein at this site. Furthermore, these data provide additional information for theorists, who can calculate the effect that changes in electrostatic field have on the transition state structure and energy. These data thus provide new physical insight that, when combined with high-resolution crystal structures and catalytic rate measurements, will lead to a more profound understanding of the function of carcinogenic mutants of Ras.

Second, and most importantly, because the dissociation constant of the Ras—Raf complex (3.5 nM)[13] is significantly lower than that of the Ras—RasGAP complex (1−100 μM),[16] any drug candidate that increases the rate of GTP hydrolysis by targeting the docking interface of Ras will be interacting with Ras when it is bound to the downstream effector, not RasGAP. The purpose of the experiments described here is not simply to report on electrostatic effects encountered by a SCN probe on the downstream effector caused by Ras Q61X mutants, but to lay the groundwork for further studies in which the effect of small molecules that interact with the Ras—effector interface and alter the rate of intrinsic Ras hydrolysis can be explored.

■ CONCLUSIONS

Here we have used VSE spectroscopy to probe electrostatic effects on protein—protein interactions in pathological Ras mutants to learn how mutations in Ras at glutamine 61 influence the function of Ras—effector interfaces. We have found that changes in the vibrational absorption energy of an appropriately placed thiocyanate probe are directly correlated to the polar surface area of side chains at position 61 of Ras. Furthermore, the vibrational absorption energy was correlated to changes in the hydration potential of all amino acid mutant side chains, although the correlation was much stronger for residues containing polar character than it was for residues containing only nonpolar functionality. These results support the hypothesis that the role of Ras Q61 is to stabilize water in or near the active site during GTP hydrolysis. This work suggests further experiments to explore the role of nonpolar residues on the absorption energy of the thiocyanate probe and the influence of Ras Q61X mutants on the rate of intrinsic GTP hydrolysis.

■ AUTHOR INFORMATION

Corresponding Author
*E-mail: lwebb@cm.utexas.edu. Phone: (512) 471-9361. Fax: (512) 471-9299.

Notes
The authors declare no competing financial interest.

■ ACKNOWLEDGMENTS

■ ABBREVIATIONS

GTP, guanosine triphosphate; GDP, guanosine diphosphate; VSE, vibrational Stark effect; RBD, Ras-binding domain; Ral, Ral guanine nucleotide dissociation stimulator; Rap, Rap1A; RasGAP, Ras GTPase-activating protein; His-TEV, histidine-tagged tobacco etch virus; GDPNP, guanosine 5′-(β,γ-imido)-triphosphate trisodium salt hydrate; DTNB, 5,5′-dithiobis(2-nitrobenzoic acid); TNB, thionitrobenzoic acid; ESI-MS, electrospray ionization mass spectrometry; GDI, guanine nucleotide dissociation inhibition; mant-GTP, 2′(or 3′)-O-(N-methylanthraniloyl)guanosine 5′-triphosphate trisodium salt; fwhm, full width at half-maximum; SASA, solvent accessible surface area.

■ REFERENCES

(1) Krauss, G. (2003) *Biochemistry of Signal Transduction and Regulation*, 3rd ed., Wiley-VCH Verlag, Weinheim, Germany.

(2) Cox, A. D., and Der, C. J. (2003) The dark side of Ras: Regulation of apoptosis. *Oncogene 22*, 8999−9006.

(3) Downward, J. (2002) Targeting Ras Signalling Pathways in Cancer Therapy. *Nat. Cancer Rev. 3*, 11−22.

(4) Repasky, G. A., Chenette, E. J., and Der, C. J. (2004) Renewing the conspiracy theory debate: Does Raf function alone to mediate Ras oncogenesis? *Trends Cell Biol. 14*, 639−647.

(5) Shields, J. M., Pruitt, K., McFall, A., Shaub, A., and Der, C. J. (2000) Understanding Ras: 'it ain't over 'til it's over'. *Trends Cell Biol. 10*, 147−154.

(6) Harvey, J. J. (1964) An Unidentified Virus which Causes the Rapid Production of Tumours in Mice. *Nature 204*, 1104−1105.

(7) Bos, J. L. (1989) ras Oncogenes in Human Cancer: A Review. *Cancer Res. 49*, 4682−4689.

(8) Eisenberg, S., and Henis, Y. I. (2008) Interactions of Ras proteins with the plasma membrane and their roles in signaling. *Cell. Signalling 20*, 31−39.

(9) Pacold, M. E., Suire, S., Perisic, O., Lara-Gonzalez, S., Davis, C. T., Walker, E. H., Hawkins, P. T., Stephens, L., Eccleston, J. F., and Williams, R. L. (2000) Crystal Structure and Functional Analysis of Ras Binding to Its Effector Phosphoinositide 3-Kinase γ. *Cell 103*, 931−943.

(10) Scheffzek, K., Ahmadian, M. R., Kabsch, W., Wiesmuller, L., Lautwein, A., Schmitz, F., and Wittinghofer, A. (1997) The Ras-RasGAP Complex: Structural Basis for GTPase Activation and Its Loss in Oncogenic Ras Mutants. *Science 277*, 333−338.

(11) Schweins, T., Geyer, M., Scheffzek, K., Warshel, A., Kalbitzer, H. R., and Wittinghofer, A. (1995) Substrate-assisted catalysis as a mechanism for GTP hydrolysis of p21ras and other GTP-binding proteins. *Nat. Struct. Biol. 2*, 36−44.

(12) Ford, B., Hornak, V., Kleinman, H., and Nassar, N. (2006) Structure of a Transient Intermediate for GTP Hydrolysis by Ras. *Structure 14*, 427−436.

(13) Buhrman, G., Holzapfel, G., Fetics, S., and Mattos, C. (2010) Allosteric modulation of Ras positions Q61 for a direct role in catalysis. *Proc. Natl. Acad. Sci. U.S.A. 107*, 4931−4936.

(14) Frech, M., Darden, T. A., Pedersen, L. G., Foley, C. K., Charifson, P. S., Anderson, M. W., and Wittinghofer, A. (1994) Role of Glutamine-61 in the Hydrolysis of GTP by p21H-Ras; An Experimental and Theoretical Study. *Biochemistry 33*, 3237−3244.

(15) Shurki, A., and Warshel, A. (2004) Why Does the Ras Switch "Break" by Oncogenic Mutations? *Proteins 55*, 1−10.

(16) Vogel, U. S., Dixon, R. A. F., Schaber, M. D., Diehl, R. E., Marshall, M. S., Scolnick, E. M., Sigal, I. S., and Gibbs, J. B. (1988) Cloning of bovine GAP and its interaction with oncogenic ras p21. *Nature 335*, 90−93.

(17) Pai, E. F., Krengel, U., Petsko, G. A., Goody, R. S., Kabsch, W., and Wittinghofer, A. (1990) Refined crystal structure of the triphosphate conformation of H-ras p21 at 1.35 Å resolution: Implications for the mechanism of GTP hydrolysis. *EMBO J. 9*, 2351−2359.

(18) Krengel, U., Schlichting, I., Scherer, A., Schumann, R., Frech, M., John, J., Kabsch, W., Pai, E. F., and Wittinghofer, A. (1990) Three-Dimensional Structures of H-ras p21 Mutants: Molecular Basis for Their Inability to Function as Signal Sitch Molecules. *Cell 62*, 539−548.

(19) Buhrman, G., Wink, G., and Mattos, C. (2007) Transformation Efficiency of RasQ61 Mutants Linked to Structural Features of the Switch Regions in the Presence of Raf. *Structure 15*, 1618−1629.

(20) Thielges, M. C., Case, D. A., and Romesberg, F. E. (2008) Carbon-Deuterium Bonds as Probes of Dihydrofolate Reductase. *J. Am. Chem. Soc. 130*, 6597−6603.

(21) Ye, S., Zaitseva, E., Caltabiano, G., Schertler, G. F. X., Sakmar, T. P., Deupi, X., and Vogel, R. (2010) Tracking G-protein-coupled receptor activation using genetically encoded infrared probes. *Nature 464*, 1386−1391.

(22) Suydam, I. T., and Boxer, S. G. (2003) Vibrational Stark Effects Calibrate the Sensitivity of Vibrational Probes for Electric Fields in Proteins. *Biochemistry 42*, 12050−12055.

(23) Webb, L. J., and Boxer, S. G. (2008) Electrostatic Fields Near the Active Site of Human Aldose Reductase: 1. New Inhibitors and Vibrational Stark Effect Measurements. *Biochemistry 47*, 1588−1598.

(24) Waegele, M. M., Culik, R. M., and Gai, F. (2011) Site-Specific Spectroscopic Reporters of the Local Electric Field, Hydration, Structure, and Dynamics of Biomolecules. *J. Phys. Chem. Lett. 2*, 2598−2609.

(25) Gunner, M. R., Nicholls, A., and Honig, B. (1996) Electrostatic Potentials in *Rhodopseudomonas viridis* Reaction Centers: Implications for the Driving Force and Directionality of Electron Transfer. *J. Phys. Chem. 100*, 4277−4291.

(26) Honig, B., and Nicholls, A. (1995) Classical Electrostatics in Biology and Chemistry. *Science 268*, 1144−1149.

(27) Lee, L. P., and Tidor, B. (2001) Optimization of Binding Electrostatics: Charge Complementarity in the Barnase-Barstar Protein Complex. *Protein Sci. 10*, 362−377.

(28) Simonson, T. (2001) Macromolecular electrostatics: Continuum models and their growing pains. *Curr. Opin. Struct. Biol. 11*, 243−252.

(29) Villa, J., and Warshel, A. (2001) Energetics and Dynamics of Enzymatic Reactions. *J. Phys. Chem. B 105*, 7887−7907.

(30) Warshel, A., and Papazyan, A. (1998) Electrostatic effects in macromolecules: Fundamental concepts and practical modeling. *Curr. Opin. Struct. Biol. 8*, 211−217.

(31) Sigala, P. A., Fafarman, A. T., Bogard, P. E., Boxer, S. G., and Herschlag, D. (2007) Do Ligand Binding and Solvent Exclusion Alter the Electrostatic Character within the Oxyanion Hole of an Enzymatic Active Site? *J. Am. Chem. Soc. 129*, 12104−12105.

(32) Fafarman, A. T., Sigala, P. A., Herschlag, D., and Boxer, S. G. (2010) Decomposition of Vibrational Shifts of Nitriles into Electrostatic and Hydrogen-Bonding Effects. *J. Am. Chem. Soc. 132*, 12811−12813.

(33) Baran, K. L., Chimenti, M. S., Schlessman, J. L., Fitch, C. A., Herbst, K. J., and Garcia-Moreno, B. E. (2008) Electrostatic Effects in a Network of Polar and Ionizable Groups in Staphylococcal Nuclease. *J. Mol. Biol. 379*, 1045−1062.

(34) Castaneda, C. A., Fitch, C. A., Majumdar, A., Khangulov, V., Schlessman, J. L., and Garcia-Moreno, B. E. (2009) Molecular determinants of the pHa values of Asp and Glu residues in staphylococcal nuclease. *Proteins 77*, 570−588.

(35) Danielson, M. A., and Falke, J. J. (1996) Use of ^{19}F NMR To Probe Protein Structure and Conformational Changes. *Annu. Rev. Biophys. Biomol. Struct. 25*, 163−195.

(36) Forsyth, W. R., Antosiewicz, J. M., and Robertson, A. D. (2002) Empirical Relationships Between Protein Structure and Carboxyl pKa Values in Proteins. *Proteins 48*, 388−403.

(37) Harms, M. J., Castaneda, C. A., Schlessman, J. L., Sue, G. R., Isom, D. G., Cannon, B. R., and Garcia-Moreno, B. E. (2009) The pKa Values of Acidic and Basic Residues Buried at the Same Internal Location in a Protein Are Governed by Different Factors. *J. Mol. Biol. 389*, 34−47.

(38) Matousek, W. M., Ciani, B., Fitch, C. A., Garcia-Moreno, B. E., Kammerer, R. A., and Alexandrescu, A. T. (2007) Electrostatic Contributions to the Stability of the GCN4 Leucine Zipper Structure. *J. Mol. Biol. 374*, 206−219.

(39) Pearson, J. G., Oldfield, E., Lee, F. S., and Warshel, A. (1993) Chemical Shifts in Proteins: A Shielding Trajectory Analysis of the Fluorine Nuclear Magnetic Resonance Spectrum of the *Escherichia coli* Galactose Binding Protein Using a Multipole Shielding Polarizability-Local Reaction Field-Molecular Dynamics Approach. *J. Am. Chem. Soc. 115*, 6851−6862.

(40) Schutz, C. N., and Warshel, A. (2001) What are Dielectric "Constants" of Proteins and How to Validate Electrostatic Models? *Proteins 44*, 400−417.

(41) Thurlkill, R. L., Grimsley, G. R., Scholtz, J. M., and Pace, C. N. (2006) Hydrogen Bonding Markedly Reduces the pKa of Buried Carboxyl Groups in Proteins. *J. Mol. Biol. 362*, 594−604.

(42) Fafarman, A. T., Webb, L. J., Chuang, J. I., and Boxer, S. G. (2006) Site-Specific Conversion of Cysteine Thiols into Thiocyanate Creates an IR Probe for Electric Fields in Proteins. *J. Am. Chem. Soc. 128*, 13356−13357.

(43) Stafford, A. J., Ensign, D. L., and Webb, L. J. (2010) Vibrational Stark Effect Spectroscopy at the Interface of Ras and Rap1A Bound to the Ras Binding Domain of RalGDS Reveals an Electrostatic Mechanism for Protein-Protein Interaction. *J. Phys. Chem. B 114*, 15331−15344.

(44) Suydam, I. T., Snow, C. D., Pande, V. S., and Boxer, S. G. (2006) Electric Fields at the Active Site of an Enzyme: Direct Comparison of Experiment with Theory. *Science 313*, 200−204.

(45) Ensign, D. L., and Webb, L. J. (2011) Factors Determining Electrostatic Fields at the Ras/Effector Interface. *Proteins 79*, 3511−3524.

(46) Huang, L., Hofer, F., Martin, G. S., and Kim, S. H. (1998) Structural basis for the interaction of Ras with RalGDS. *Nat. Struct. Biol. 5*, 422−426.

(47) Rudolph, M. G., Linnemann, T., Grunewald, P., Wittinghofer, A., Vetter, I. R., and Herrmann, C. (2001) Thermodynamics of Ras/Effector and Cdc42/Effector Interactions Probed by Isothermal Titration Calorimetry. *J. Biol. Chem. 276*, 23914−23921.

(48) Kapust, R. B., Tozser, J., Fox, J. D., Anderson, D. E., Cherry, S., Copeland, T. D., and Waugh, D. S. (2001) Tobacco etch virus protease: Mechanism of autolysis and rational design of stable mutants with wild-type catalytic proficiency. *Protein Eng. 14*, 993−1000.

(49) Boriack-Sjodin, P. A., Margarit, S. M., Bar-Sagi, D., and Kuriyan, J. (1998) The structural basis of the activation of Ras by Sos. *Nature 394*, 337−343.

(50) Herrmann, C., Horn, G., Spaargaren, M., and Wittinghofer, A. (1996) Differential Interactions of the Ras Family of GTP-binding Proteins H-Ras, Rap1A, and R-Ras with the Putative Effector Molecules Raf Kinase and Ral-Guanine Nucleotide Exchange Factor. *J. Biol. Chem. 271*, 6794−6800.

(51) Choi, J. H., Oh, K. I., Lee, H., Lee, C., and Cho, M. (2008) Nitrile and thiocyanate IR probes: Quantum chemistry calculation studies and multivariate least-square fitting analysis. *J. Chem. Phys. 128*, 134506.

(52) Duan, Y., Wu, C., Chowdhury, S., Lee, M. C., Xiong, G., Zhang, W., Yang, R., Cieplak, P., Luo, R., Lee, T., Caldwell, J. W., Wang, J., and Kollman, P. A. (2003) A Point-Charge Force Field for Molecular Mechanics Simulations of Proteins Based on Condensed-Phase Quantum Mechanical Calculations. *J. Comput. Chem. 24*, 1999−2012.

(53) van der Spoel, D., Lindahl, E., Hess, B., Groenhof, G., Mark, A. E., and Berendsen, H. J. C. (2005) GROMACS: Fast, Flexible, and Free. *J. Comput. Chem. 26*, 1701−1718.

(54) Jorgensen, W. L., Chandrasekhar, J., Madura, J. D., Impey, R. W., and Klein, M. L. (1983) Comparison of simple potential functions for simulating liquid water. *J. Chem. Phys. 79*, 926−935.

(55) Gallicchio, E., Andrec, M., Felts, A. K., and Levy, R. M. (2005) Temperature Weighted Histogram Analysis Method, Replica Exchange, and Transition Paths. *J. Phys. Chem. B 109*, 6722−6731.

(56) Roux, B. (1995) The calculation of the potential of mean force using computer simulations. *Comput. Phys. Commun. 91*, 275−282.

(57) Wimley, W. C., Creamer, T. P., and White, S. H. (1996) Solvation Energies of Amino Acid Side Chains and Backbone in a Family of Host-Guest Pentapeptides. *Biochemistry 35*, 5109−5124.

(58) Wolfenden, R., Andersson, L., Cullis, P. M., and Southgate, C. C. B. (1981) Affinities of Amino Acid Side Chains for Solvent Water. *Biochemistry 20*, 849−855.

(59) John, J., Frech, M., and Wittinghofer, A. (1988) Biochemical Properties of Ha-ras Encoded p21 Mutants and Mechanis of the Autophosphorylation Reaction. *J. Biol. Chem. 263*, 11792−11799.

(60) Leupold, C. M., Goody, R. S., and Wittinghofer, A. (1983) Stereochemistry of the elongation factor Tu-GTP complex. *Eur. J. Biochem. 135*, 237−241.

(61) Reinstein, J., Schlichting, I., Frech, M., Goody, R. S., and Wittinghofer, A. (1991) p21 with a Phenylalanine 28 to Leucine Mutation Reacts Normally with the GTPase Activating Protein GAP but Nevertheless Has Transforming Properties. *J. Biol. Chem. 266*, 17700−17706.

(62) Der, C. J., Finkel, T., and Cooper, G. M. (1986) Biological and Biochemical Properties of Human rasH Genes Mutated at Codon 61. *Cell 44*, 167−176.